

Effects of medium-induced $\rho - \omega$ meson mixing on the equation of state in isospin-asymmetric nuclear matter

Wei-Zhou Jiang^{1,2,3} and Bao-An Li¹

¹ *Department of Physics and Astronomy,*

Texas A&M University-Commerce, Commerce, TX 75429, USA

² *Department of Physics, Southeast University, Nanjing 211189, China and*

³ *Institute of Applied Physics, Chinese Academy of Sciences, Shanghai 201800, China*

(Dated:)

We reexamine effects of the $\rho - \omega$ meson mixing mediated by nucleon polarizations on the symmetry energy in isospin-asymmetric nuclear matter. Taking into account the rearrangement term neglected in previous studies by others, we evaluate the $\rho - \omega$ mixing angle in a novel way within the Relativistic Mean-Field Models with and without chiral limits. It is found that the symmetry energy is significantly softened at high densities contrary to the finding in earlier studies. As the first step of going beyond the lowest-order calculations, we also solve the RPA equation for the $\rho - \omega$ mixing. In this case, it is found that the symmetry energy is not only significantly softened by the $\rho - \omega$ mixing at supra-saturation densities, similar to the lowest-order $\rho - \omega$ mixing, but interestingly also softened at subsaturation densities. In addition, the softening of the symmetry energy at subsaturation densities can be partly suppressed by the nonlinear self-interaction of the σ meson.

PACS numbers: 21.65.+f, 11.30.Er, 11.30.Qc, 11.30.Rd

I. INTRODUCTION

Many hadronic and partonic approaches have been used in studying the charge symmetry breaking (CSB) and its effect on few-body and bulk-matter observables, see, e.g., refs. [1, 2] for reviews. The CSB effect can be displayed in the charge-conjugate systems such as the proton-proton and neutron-neutron binary systems whose scattering lengths in the 1S_0 state: a_{nn} and a_{pp} differ by 10% after deducting the electromagnetic interaction. The CSB can also be used to explain the well-known Nolen-Schiffer anomaly of light mirror nuclei. Among the hadronic approaches, the CSB effect has been incorporated into the many-body theories by employing explicitly charge-dependent nucleon-nucleon interactions, e.g., the Bonn[3], Reid93[4] and V18 potentials [5]. These interactions have been adjusted to reproduce the free-space nucleon-nucleon scattering data. However, the CSB effects in free-space and/or symmetric nuclear matter are normally very small. For example, the CSB-induced effects in symmetric nuclear matter with the charge-dependent Bonn potential were shown to be quite small [3]. The results with the charge-dependent Reid93 potential also showed that the CSB effect on the equation of state (EOS) even in isospin-asymmetric nuclear matter is negligible [4].

To explore the possible CSB mechanisms at the hadronic level, the $\rho^0 - \omega$ meson mixing (ROM) [6–11] and the hadron mass splitting effects [3, 12] have also been studied extensively. Within the meson

mixing picture, the two charge neutral vector mesons undertake a transition to each other through a baryon-antibaryon polarization. An essential point is the incomplete cancellation between the opposite contributions from proton and neutron loops to the transition amplitude [8]. In nuclear medium, the polarization acquires an overwhelming enhancement through the particle-hole excitations. Very interestingly, the ROM gets significantly amplified in isospin-asymmetric nuclear matter, see, e.g., refs. [10, 13, 14], because of the different numbers of neutrons and protons available. In a nutshell, the different stacking of protons and neutrons in the Fermi sea becomes a naissant factor to intrigue the CSB in isospin-asymmetric nuclear matter due to the medium-induced ROM. Loosely, we may call this the in-medium CSB.

The ROM in asymmetric nuclear matter also results in significant modifications to properties of the isovector meson ρ and its couplings with nucleons [9–11, 13, 14]. Since the potential part of the nuclear symmetry energy is dictated by the exchange of ρ mesons, at least within the Relativistic Mean-Field (RMF) models, corresponding modifications to the density dependence of the symmetry energy are thus expected. While most earlier studies [10, 11, 15–17] have focused on investigating the in-medium meson spectra, a few studies [13, 14] have indeed looked at effects of the medium-induced ROM on the symmetry energy. It was found that the ρ – ω mixing angle reaches its maximum of about 45° in isospin-asymmetric nuclear matter. Moreover, the symmetry energy was sharply stiffened at supra-normal densities. However, the rearrangement term, which is crucial for the thermodynamic consistency in deriving the pressure, was neglected in these RMF studies [13, 14]. We find that the rearrangement term actually causes the pressure to exceed the energy density when the mixing angle θ is close to 45° . This certainly violates the causality, namely, the work done by the pressure of the system should be less than its total energy. In this work, using the RMF Lagrangian constructed by us recently [18, 19] including constraints of a mass dropping scenario according to the Brown-Rho (BR) scaling [20–24], we calculate the ρ – ω mixing angle in asymmetric matter in a novel way. We then examine effects of the medium-induced ROM on the in-medium masses of the ρ and ω mesons and the density dependence of the symmetry energy. As the first step of going beyond the lowest-order nucleon polarization, we also evaluate the ρ – ω mixing within the random phase approximation (RPA). Results from the two different levels of approximations will be compared with each other. Moreover, in order to examine the model dependence we also perform the calculations with the nonlinear RMF model.

The paper is organized as follows. In Section II, we introduce the medium-induced ROM within the RMF model and the novel way to obtain the ρ – ω mixing angle. We then summarize briefly the formalisms for the ROM within both the lowest-order nucleon polarization and the RPA. Results and discussions are presented in Section III. A summary is given in Section IV.

II. MEDIUM-INDUCED $\rho - \omega$ MESON MIXING WITHIN THE RMF MODEL

The following lagrangian with the chiral limit serves as the starting point [18, 19]:

$$\begin{aligned} \mathcal{L} = & \bar{\psi}[i\gamma_\mu\partial^\mu - M + g_\sigma^*\sigma - G_\omega^*\gamma_\mu V_\omega^\mu - G_\rho^*\gamma_\mu\tau_3 V_\rho^\mu]\psi \\ & + \frac{1}{2}(\partial_\mu\sigma\partial^\mu\sigma - m_\sigma^{*2}\sigma^2) - \frac{1}{4}F_{\mu\nu}F^{\mu\nu} + \frac{1}{2}m_0^{*2}V_{\omega\mu}V_\omega^\mu \\ & - \frac{1}{4}B_{\mu\nu}B^{\mu\nu} + \frac{1}{2}m_1^{*2}V_{\rho\mu}V_\rho^\mu + \epsilon V_{\omega\mu}V_\rho^\mu \end{aligned} \quad (1)$$

where ψ, σ, V_ω , and V_ρ are the fields of the nucleon, scalar, vector, and isovector-vector mesons, with their masses M, m_σ^*, m_0^* , and m_1^* , respectively. The meson coupling constants and masses with asterisks denote the density dependence, given by the BR scaling with well restrained forms and parameters [18, 19]. We note that the BR scaling is still a phenomenological ansatz to mimic the properties of the partial restoration of the chiral symmetry although QCD-based effective field theories and models support the mass dropping scenario. For instance, as an effective QCD field theory, the hidden local symmetry theory has been developed to include the ρ meson in addition to the pion in the framework of the chiral perturbative theory by Harada and Yamawaki and it is shown that the ρ meson becomes massless at the chiral limit [23, 24]. Moreover, the controversy of the BR scaling is still unsettled by recent experiments [21], also see the discussions in Ref. [18]. Here we resort to the mass dropping scenario according to the BR scaling mainly due to its simplicity.

The term $\epsilon V_{\omega\mu}V_\rho^\mu$ in the lagrangian that mixes the isoscalar and isovector mesons breaks the charge symmetry in the isospin space. In the free space, the parameter ϵ represents the amplitude of the fundamental CSB within the ROM picture. In isospin-asymmetric nuclear matter, since the medium effect is dynamically induced, it can be conveniently expressed as

$$\epsilon = m_0^* m_1^* \gamma, \quad (2)$$

in terms of a dimensionless parameter γ . The symmetry breaking term can be exorcized at the cost of introducing a mixing angle with the unitary transformation [9, 25]:

$$V_\omega = b_0 \sin \theta + \omega \cos \theta, \quad V_\rho = b_0 \cos \theta - \omega \sin \theta, \quad (3)$$

with

$$\tan 2\theta = \frac{2\epsilon}{m_1^{*2} - m_0^{*2}}. \quad (4)$$

The lagrangian thus becomes

$$\begin{aligned} \mathcal{L} = & \bar{\psi}[i\gamma_\mu\partial^\mu - M + g_\sigma^*\sigma - g_\omega^*\gamma_\mu\omega^\mu - g_\rho^*\gamma_\mu\tau_3 b_0^\mu]\psi \\ & + \frac{1}{2}(\partial_\mu\sigma\partial^\mu\sigma - m_\sigma^{*2}\sigma^2) - \frac{1}{4}F_{\mu\nu}F^{\mu\nu} + \frac{1}{2}m_\omega^{*2}\omega_\mu\omega^\mu \\ & - \frac{1}{4}B_{\mu\nu}B^{\mu\nu} + \frac{1}{2}m_\rho^{*2}b_{0\mu}b_0^\mu, \end{aligned} \quad (5)$$

where both g_ω^* and g_ρ^* couple differently to the proton and neutron [9]:

$$g_{p\omega}^* = G_\omega^* \cos \theta - G_\rho^* \sin \theta, \quad g_{n\omega}^* = G_\omega^* \cos \theta + G_\rho^* \sin \theta \quad (6)$$

$$g_{p\rho}^* = G_\rho^* \cos \theta + G_\omega^* \sin \theta, \quad g_{n\rho}^* = G_\rho^* \cos \theta - G_\omega^* \sin \theta \quad (7)$$

The ω and ρ masses are given by

$$\begin{aligned} m_\omega^{*2} &= \frac{m_0^{*2} + m_1^{*2}}{2} + \frac{m_0^{*2} - m_1^{*2}}{2 \cos 2\theta}, \\ m_\rho^{*2} &= \frac{m_0^{*2} + m_1^{*2}}{2} - \frac{m_0^{*2} - m_1^{*2}}{2 \cos 2\theta}, \end{aligned} \quad (8)$$

where the masses of ρ and ω mesons shift oppositely with θ , required by the transformational unitarity in Eq.(3). The energy density, based on Eq.(5), reads,

$$\begin{aligned} \mathcal{E} &= \frac{(g_{p\omega}^* \rho_p + g_{n\omega}^* \rho_n)^2}{2m_\omega^{*2}} + \frac{(g_{p\rho}^* \rho_p - g_{n\rho}^* \rho_n)^2}{2m_\rho^{*2}} \\ &\quad + \frac{1}{2} m_\sigma^{*2} \sigma^2 + \sum_{i=p,n} \frac{2}{(2\pi)^3} \int_0^{k_{Fi}} d^3k E_i^*, \end{aligned} \quad (9)$$

where the θ is embedded in both meson masses and their couplings to nucleons. Given the $\rho - \omega$ meson mixing by the nucleon polarization that is beyond the mean field, the rearrangement term is inevitably induced to keep the Lorentz invariance of the RMF model. This is a general case in the density-dependent RMF models where the density dependence is incorporated beyond the mean field, e.g., see [18, 19, 26]. Besides the contribution from the BR scaling, the density-dependent mixing angle results in a new source of the rearrangement term in the pressure

$$\begin{aligned} p &= \frac{(g_{p\omega}^* \rho_p + g_{n\omega}^* \rho_n)^2}{2m_\omega^{*2}} + \frac{(g_{p\rho}^* \rho_p - g_{n\rho}^* \rho_n)^2}{2m_\rho^{*2}} \\ &\quad - \frac{1}{2} m_\sigma^{*2} \sigma^2 - \Sigma_0 \rho + \frac{1}{3} \sum_{i=p,n} \frac{2}{(2\pi)^3} \int_0^{k_{Fi}} d^3k \frac{\mathbf{k}^2}{E_i^*}. \end{aligned} \quad (10)$$

Here, an additional θ -related part $-\partial\mathcal{E}/\partial\theta \cdot \partial\theta/\partial\rho$ neglected in Refs. [13, 14] makes the rearrangement term Σ_0 more involved than that in Ref. [18], and the final result is obtained numerically.

A key point is to derive the $\rho - \omega$ mixing angle through the nucleon polarization. In principle, one can firstly determine the ROM parameter ϵ or γ directly from the polarization with the relation $g_{\mu\nu}\epsilon = \Pi_{\mu\nu}^{\rho\omega}(q^2)$ according to the lagrangian (1), similar to the case in the free space [8], and then the mixing angle can be obtained through Eq.(4). However, the ROM parameters ϵ and γ obtained in this way have a complicated structure in momentum space [8]. In order to obtain momentum-independent ROM parameters in the mean-field approximation, an average procedure is necessary. As mentioned in the Introduction, the mixing angle obtained with such an averaging procedure in Refs. [13, 14] is large enough to cause the violation of causality. Here, we pursue a new approach. We

first evaluate the total energy density from the lagrangian (1) but with the explicit ROM replaced by the polarization diagram in bulk matter, see Fig. 1. Since the polarization diagram is a contribution beyond the RMF approach, the polarization in Fig. 1 is not limited only to its temporal component considered in Refs. [13, 14]. The ROM angle appearing in the lagrangian (5) is then determined by reproducing this total energy density using Eq.(9). Meanwhile, the ROM parameter ϵ or γ can be calculated through Eq.(4). Nevertheless, here we indeed evaluate the ROM parameter ϵ in the lagrangian (1) through the $\rho^0 - \omega$ transition amplitude. In isospin-asymmetric matter, the medium effect is dynamically induced due to the incomplete cancellation of the proton and neutron loops. In the lowest order of the meson-nucleon coupling, this is equivalent to computing the contribution of the lowest-order nucleon polarizations to the energy density. To include the high-order effect, we need to solve the RPA (Dyson) equation to sum up relevant nucleon loops to all orders.

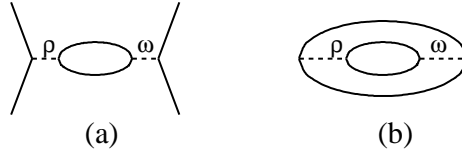


FIG. 1: Diagrams for (a) the scattering, and (b) the corresponding contribution to the potential energy density.

The energy density can be written quite generally as [27–29] $\mathcal{E} = \mathcal{T} + \mathcal{V}/2$, where the \mathcal{T} and \mathcal{V} are the kinetic and potential parts, respectively. The polarization diagram gives rise to a term \mathcal{V}' adding to the potential energy density \mathcal{V} . Considering \mathcal{V}' is just a few percents compared to the vector potential even in pure neutron matter, we neglect its direct correction to the meson fields (or, nucleon self-energies) that are solved in the RMF equations. In fact, a full calculation with the meson fields including this term brings about the momentum dependence of the nucleon potential which should be fulfilled at least in the Hartree-Fock (HF) framework. This is, however, beyond the present RMF treatment. In the evaluation of the \mathcal{V}' , the polarization tensor is wrapped up by the nucleon current only in the Fermi sea. This approach is actually widely used in the study of bulk matter [27–29]. The \mathcal{V}' is thus written as

$$\begin{aligned} \mathcal{V}' &= -G_\omega^* G_\rho^* \int \frac{d^3 p_1}{(2\pi)^3} \frac{d^3 p_2}{(2\pi)^3} \text{Tr} \left[\frac{\not{p}_1^* + M_i^*}{2E_{p_1 i}^*} \gamma^\mu \tau_3 \frac{\not{p}_2^* + M_i^*}{2E_{p_2 i}^*} \gamma^\nu \right] \\ &\quad \times \frac{\Pi_{\mu\nu}^{\rho\omega}(q)}{(m_0^{*2} - q^2)(m_1^{*2} - q^2)}, \end{aligned} \quad (11)$$

where $p_i^{*0} = E_{p_i}^* = \sqrt{\mathbf{p}^2 + M_i^{*2}}$, $\mathbf{q} = \mathbf{p}_2 - \mathbf{p}_1$ and $q_0 = E_{p_2}^* - E_{p_1}^*$. The polarization tensor is given by

$$\Pi_{\mu\nu}^{\rho\omega}(q) = -iG_\omega^* G_\rho^* \int \frac{d^4 k}{(2\pi)^4} \text{Tr} [\gamma_\mu G(k) \gamma_\nu \tau_3 G(k+q)], \quad (12)$$

where $G(k)$ is the nucleon propagator, and the trace is over both the isospin (τ) and spin (γ) matrices. Here, the polarization tensor is given in the lowest order, while the high-order corrections will be considered later on by solving the RPA (Dyson) equation. As seen in Eq.(11), only the real part of the polarization is needed to evaluate the \mathcal{V}' . Usually, the imaginary part concerns the stability of the mean field in small oscillations. Indeed, it also comes into play in the real part of the polarization by taking into account the high-order corrections in the RPA equation. First of all, we consider the case with the lowest-order polarization. By choosing the frame $(q_0, \bar{q}, 0, 0)$ with $q^2 = q_0^2 - \bar{q}^2$, one can define the longitudinal (L) and transverse (T) components [30]:

$$\Pi_L = \Pi_{33} - \Pi_{00}, \quad \Pi_T = \Pi_{11} = \Pi_{22}. \quad (13)$$

In free space $\Pi_L = \Pi_T = \Pi^F(q^2)$. Here, the tensor coupling constant of ρ meson is not included because it is in principle nonrenormalizable. In the medium, the polarization tensor is usually decomposed into Feynman and density-dependent parts: $\Pi = \Pi^F + \Pi^D$, while the former is just the one in free space but with the in-medium nucleon mass. The trace over the isospin makes the Feynman parts of the proton and neutron polarizations to cancel each other, leading to [8]

$$\Pi^{\rho\omega, F}(q^2) = \frac{q^2}{2\pi^2} G_\omega^* G_\rho^* \int_0^1 dx x(1-x) \ln \frac{M_p^{*2} - x(1-x)q^2}{M_n^{*2} - x(1-x)q^2}. \quad (14)$$

In the medium, the longitudinal and transverse components of the density-dependent part are not equal [30]:

$$\begin{aligned} \Pi_L^{\rho\omega, D} &= -8q^2 G_\omega^* G_\rho^* \sum_{i=p,n} s \int \frac{d^3k}{(2\pi)^3} \frac{\Theta(k_{F_i} - |k|)}{E_{ki}^*} \frac{E_{ki}^{*2} - \mathbf{k}^2 \chi^2}{(q^2)^2 - 4(k \cdot q)^2} \\ \Pi_T^{\rho\omega, D} &= -8G_\omega^* G_\rho^* \sum_{i=p,n} s \int \frac{d^3k}{(2\pi)^3} \frac{\Theta(k_{F_i} - |k|)}{E_{ki}^*} \frac{q^2 \mathbf{k}^2 (\chi^2 - 1)/2 + (k \cdot q)^2}{(q^2)^2 - 4(k \cdot q)^2}, \end{aligned} \quad (15)$$

where Θ is the step function, k_{F_i} with $i = p, n$ are respectively the proton and neutron Fermi momenta, $k \cdot q = E_{ki}^* q_0 - |\mathbf{k}| \bar{q} \chi$, $\chi = \cos \angle \mathbf{k} \cdot \mathbf{q}$, and $s = \pm 1$ for proton and neutron, respectively. Note that only the real parts of the polarization are given here. With the chosen frame for q_μ , the polarization can be written as:

$$\begin{aligned} \Pi_{\mu\nu}^D &= (-g_{\mu\nu} + q_\mu q_\nu / q^2) \Pi_L^D, \quad \mu, \nu = 3, 0 \\ \Pi_{\mu\nu}^D &= -g_{\mu\nu} \Pi_T^D, \quad \mu, \nu = 1, 2. \end{aligned} \quad (16)$$

Substituting Eqs.(14),(16) in (11) and considering the conservation of baryon number, we obtain

$$\begin{aligned} \mathcal{V}' &= \frac{4G_\omega^* G_\rho^*}{(2\pi)^4} \sum_{i=p,n} s \int_0^{k_{F_i}} p_1^2 p_2^2 dp_1 dp_2 \int_{-1}^1 d\chi_p \left\{ \frac{p_1 p_2 \chi_p + M_i^{*2}}{E_{p_1 i}^* E_{p_2 i}^*} \Pi_L^{\rho\omega}(q) \right. \\ &\quad \left. + \left(\frac{M_i^{*2}}{E_{p_1 i}^* E_{p_2 i}^*} - 1 \right) \Pi_T^{\rho\omega}(q) \right\} \frac{1}{(m_0^{*2} - q^2)(m_1^{*2} - q^2)}, \end{aligned} \quad (17)$$

with $\chi_p = \cos \angle \mathbf{p}_1 \cdot \mathbf{p}_2$. With this expression that surrogates the explicit ROM, we can obtain straightforwardly the total energy density from the lagrangian (1) in the RMF approximation.

In the above, we calculated the additional energy density from the lowest-order polarization of the ROM without including the high-order ones. A more elaborate treatment needs to include the ROM and the high-order corrections altogether by solving the RPA equation. The RPA equation for the polarizations is given as:

$$\tilde{\Pi}_{\mu\nu} = \Pi_{\mu\nu} + \tilde{\Pi}_{\mu\lambda} \mathcal{D}^{\lambda\tau} \Pi_{\tau\nu}. \quad (18)$$

This equation can be decomposed into the longitudinal and transverse parts as

$$\begin{aligned} \tilde{\Pi}_T &= \Pi_T + \tilde{\Pi}_T \mathcal{D}_T \Pi_T, \\ \tilde{\Pi}_L &= \Pi_L + \tilde{\Pi}_L \mathcal{D}_L \Pi_L, \end{aligned} \quad (19)$$

where the lowest-order polarization matrices are given as:

$$\Pi_T = \begin{pmatrix} \Pi_T^{\omega\omega} & \Pi_T^{\rho\omega} \\ \Pi_T^{\rho\omega} & \Pi_T^{\rho\rho} \end{pmatrix}, \quad \Pi_L = \begin{pmatrix} \Pi_0^{\sigma\sigma} & \Pi_0^{\sigma\omega} & \Pi_0^{\sigma\rho} \\ \Pi_0^{\sigma\omega} & \Pi_0^{\omega\omega} & \Pi_0^{\omega\rho} \\ \Pi_0^{\sigma\rho} & \Pi_0^{\omega\rho} & \Pi_0^{\rho\rho} \end{pmatrix}, \quad (20)$$

and the meson propagator matrices are diagonal [31, 32]

$$\mathcal{D}_T = \begin{pmatrix} D_\omega & 0 \\ 0 & D_\rho \end{pmatrix}, \quad \mathcal{D}_L = \begin{pmatrix} \Delta & 0 & 0 \\ 0 & q^2 D_\omega / \bar{q}^2 & 0 \\ 0 & 0 & q^2 D_\rho / \bar{q}^2 \end{pmatrix}, \quad (21)$$

with $\Delta = 1/(q^2 - m_\sigma^2 + i\varepsilon)$, and $D_{\omega,\rho} = 1/(q^2 - m_{0,1}^2 + i\varepsilon)$. Now, the polarizations of the ROM in the RPA can be written explicitly as:

$$\tilde{\Pi}_L^{\rho\omega} = \frac{q^2}{\bar{q}^2} \tilde{\Pi}_{00}^{\rho\omega} = \frac{\Pi_L^{\rho\omega} + \Delta \left(\frac{q^2}{\bar{q}^2} \Pi_0^{\sigma\omega} \Pi_0^{\sigma\rho} - \Pi^{\sigma\sigma} \Pi_L^{\rho\omega} \right)}{\epsilon_L}, \quad \tilde{\Pi}_T^{\rho\omega} = \frac{\Pi_T^{\rho\omega}}{\epsilon_T}, \quad (22)$$

where the dielectric functions ϵ_L and ϵ_T are the determinants of the matrices $(1 - \mathcal{D}_L \Pi_L)$ and $(1 - \mathcal{D}_T \Pi_T)$, respectively. Their explicit expressions, together with definitions of the polarizations in matrices (20), are given in appendix A. Note that the imaginary parts of the polarizations are also included in the RPA equation, and thus finally we take the real part of the $\tilde{\Pi}^{\rho\omega}$ in the calculation of the energy density. Here, except for $\Pi^{\rho\omega}$, the vacuum part is neglected for all other polarizations since we work in the RMF approximation. Substituting above expressions into Eq.(17), we may evaluate the additional energy density within the RPA.

III. RESULTS AND DISCUSSIONS

Our numerical calculations are carried out based on the SLC [19] and the well-known NL3 [33] parameter sets. The SLC parameter set was obtained by reproducing the pressure profile constrained

at supra-saturation densities by the collective flow data from relativistic heavy-ion reactions [34] and the density dependence of the symmetry energy at subsaturation densities obtained from studying isospin diffusion in heavy-ion reactions at intermediate energies [35–37], besides the saturation properties of nuclear matter. In the following, we first carry out numerical calculations within the lowest-order ROM picture. This facilitates easy and direct comparisons with earlier studies by others [13, 14]. In this case, the retardation effect is neglected by taking $q_0 = 0$ as in many other calculations [27–29]. This makes the calculations much easier. The small difference in proton and neutron masses is retained in our calculations. To go beyond the lowest-order ROM, we have also re-calculated all key quantities using the RPA. Results of these calculations will be compared with those using the lowest-order ROM.

A. Results with the lowest-order ROM

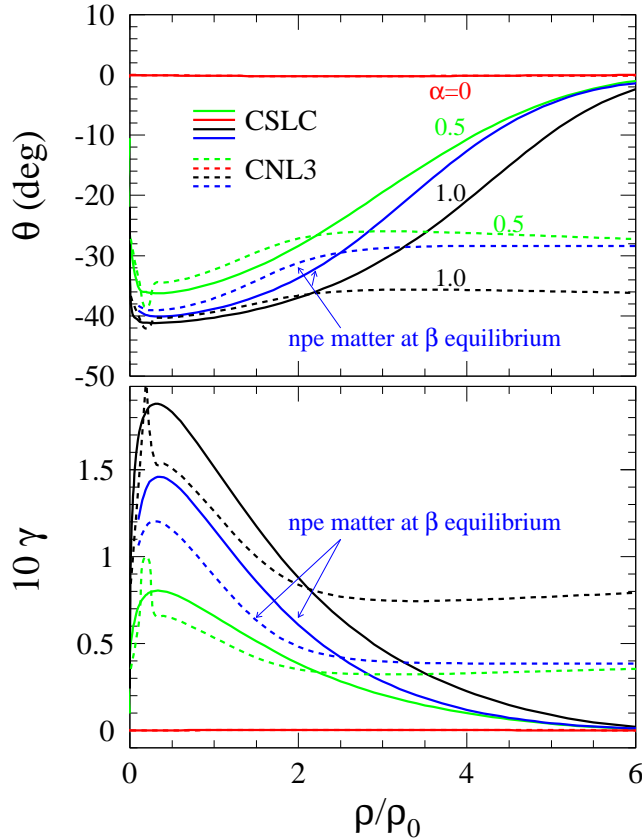


FIG. 2: (Color online) The mixing angle (the upper panel) and the parameter γ (the lower panel) as a function of density for different isospin asymmetries and npe matter at β equilibrium with the CSLC and CNL3.

The $\rho - \omega$ mixing angle is obtained by reproducing the total energy density including the polarization diagram as we outlined in the previous section. Fig. 2 depicts the $\rho - \omega$ mixing angle θ and the

dimensionless parameter γ for different isospin asymmetries $\alpha = (\rho_n - \rho_p)/\rho_B$ as a function of density with the CSLC (solid lines) and CNL3 (dashed lines). The model CSLC is simply the model SLC plus the in-medium CSB given by the ROM. Since the in-medium CSB is negligible in symmetric matter, both the CSLC and SLC have almost the same EOS for symmetric matter. In order to have the same $E_{\text{sym}} = 31.6$ MeV at saturation density $\rho_0 = 0.16 \text{ fm}^{-3}$ [36, 37] as the SLC, G_ρ (i.e., G_ρ^* at $\rho = 0$) in the CSLC is readjusted to 2.82. Similarly, the model CNL3 is constructed from the original model NL3 plus the in-medium CSB but with $G_\rho = 3.02$ to have the same symmetry energy at saturation density as given by the NL3. The θ is negative which is opposite to that in Refs. [13, 14] where only the temporal component of the polarization was considered. Our result is consistent with that in Ref. [10] where the θ was obtained from accounting higher-order contributions in the Dyson equation. In free space, the θ goes to zero in our calculation because the observed energy density, actually obtained by subtracting the vacuum expectation value, is zero in the free space. The mixing angle is negligibly small for $\alpha = 0$, and increases with α as one expects. For pure neutron matter, the magnitude of the θ reaches the maximum value of about 40° at very low densities and then decreases with the increasing density. Since neutron stars are among the most neutron-rich and mysterious objects in the Universe, it is interesting to also examine the mixing angle in the neutron-proton-electron (npe) matter at β equilibrium. As shown also in Fig. 2, the mixing angle in the npe matter at β equilibrium is generally between those for pure neutron matter and $\alpha = 0.5$. The γ , shown in the lower panel of Fig. 2, varies from almost zero in symmetric matter to about 0.2 in highly isospin-asymmetric matter at low densities, while at high densities it decreases with the CSLC and almost saturates with the CNL3, similar to the mixing angle θ . We stress here that in all cases considered, the mixing angle is negative with its magnitude well below 45° . This is rather different from that obtained in Refs. [13, 14]. We can thus avoid naturally the unphysical result that the ρ -meson mass becomes imaginary when the magnitude of θ is close to 45° as seen in Eq.(8).

The nuclear EOS obtained with the SLC differs mainly in the high density region from that with the NL3. The latter also has no nonlinear terms for vector mesons and thus guarantees the simplicity of the linear transformation in Eq.(3). It is thus interesting to compare their predictions on the mixing angles. First of all, it is seen from Fig. 2 that the maximum magnitude of the mixing angle with the CNL3 is also well below 45° . Secondly, it is seen that the difference between predictions with the CSLC and CNL3 is mainly at high densities. While the CNL3 predicts approximately constant and large mixing angles, the values with the CSLC become almost zero at high densities. This is understandable since the mixing angle is originated from the nucleon polarization. In the CSLC, the vertices from the polarization are dictated by the BR scaling that plays an important role in suppressing the medium-induced ROM contribution as seen in the Eq.(17) and Fig. 1. In the

CNL3, however, such a suppressing factor does not exist. Therefore, there is a large difference in the predicted mixing angle. The difference for the parameter γ between the CSLC and CNL3, shown in Fig. 2, can be understood similarly.

We now turn to the effects of the medium-induced ROM on properties of vector mesons in asymmetric matter. As an example, we consider the npe matter at β equilibrium. Fig. 3 displays the changes of the vector meson masses versus density in the npe matter at β equilibrium for the CSLC (upper window) and CNL3 (lower window) models. To separate effects due to the medium-induced ROM from those due to the mass dropping scenario, we plot separately the ρ and ω meson masses scaled by their respective masses in symmetric matter in the main frame, and the masses scaled by their respective masses in vacuum in the CSLC case, which are in fact the BR scaling functions for the meson masses [18], in the inset of the upper window. It is seen that the relatively large modification occurs mainly within the low density region. Similar to the high density behaviors of the mixing angle with the CSLC and CNL3, for the same reason the two models predict slightly different masses at high densities. With the CNL3, the splitting of the scaled ρ and ω masses stays almost unchanged at high densities, whereas with the CSLC the splitting vanishes quickly. Nevertheless, the modifications to the scaled masses are quite small and remain at the level of about 5 percent or less for both models.

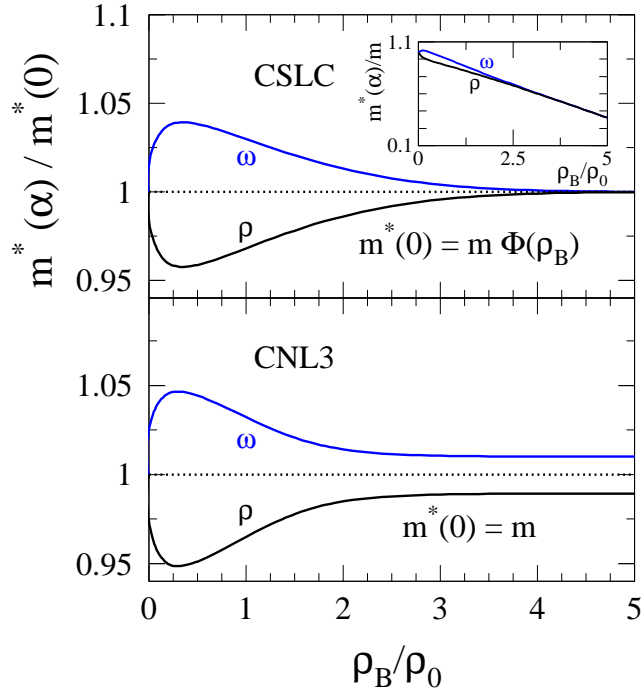


FIG. 3: (Color online) The ρ and ω meson masses in the npe matter at β equilibrium scaled by their respective masses in symmetric matter. The inset shows their masses scaled by their respective masses in vacuum. $\Phi(\rho_B)$ is the scaling function of meson masses [18].

The mass dropping relative to its vacuum value is a manifestation of the partial restoration of chiral symmetry, as suggested in many effective QCD theories. It is worthwhile to mention that some evidences for the dropping meson masses was found from studying the dilepton spectra observed at the CERN SPS [22, 38] in the 90's. Recently, a downward shift of the ω meson mass was observed at the KEK [39] and the ELSA-Bonn [40]. At saturation density, the mass ratios ($m_i^*(\alpha)/m_i(0)$, $i = \rho, \omega$) with the CSLC are predicted in the npe matter at β equilibrium ($\alpha = 0.92$) to be 0.846 and 0.9 for the ρ and ω mesons, respectively. At $\alpha = 0.2$ which is approximately the average isospin asymmetry for the ^{208}Pb nucleus, the scaled masses at saturation density are 0.878 and 0.87 for the ρ and ω mesons, respectively. This is equivalent to a splitting of their in-medium peaks by about 17 MeV.

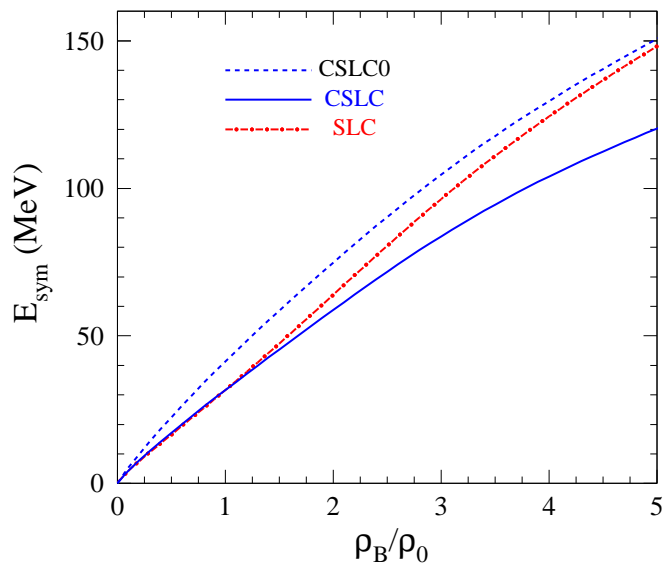


FIG. 4: (Color online) The symmetry energy as a function of density for three cases (see text).

To examine effects of the medium-induced ROM on the symmetry energy defined as $E_{sym}(\rho) \equiv (\frac{\partial^2 \mathcal{E}}{\partial \alpha^2})_\rho / 2\rho$, we compare in Fig. 4 results for three cases: the SLC, CSLC0 (SLC plus the additional energy density with the medium-induced ROM), and the CSLC. Though this additional energy density is negligible in symmetric matter, it becomes important in isospin-asymmetric matter. Consequently, the symmetry energy reflecting the cost to go away from symmetric matter is significantly modified. It is seen that the effect on the symmetry energy is significant at densities around $1 - 2\rho_0$. At higher densities, the modification fades away because the vector meson coupling constants (see Eq.(17)) tends to zero at high densities according to the BR scaling [18]. To see more clearly the influence of the medium-induced ROM on the density dependence of the symmetry energy, we also compare results obtained with the SLC and CSLC. It is interesting to see that a large softening effect is observed at high densities. While considerable progress has been made recently in constraining the density dependence of the symmetry energy at subsaturation densities using data from heavy-ion

reactions [35–37], experimental information about the symmetry energy at supra-normal densities just starts to emerge[41, 42]. The effect of the medium-induced ROM observed here is significant. It further adds to the importance to determine experimentally the symmetry energy at supra-normal densities. Hopefully, heavy-ion reactions induced by high energy radioactive beams will make this possible in the near future [43].

Now, let’s understand the in-medium CSB more clearly. Firstly, the effects of the in-medium CSB are related to the modification to the symmetry energy. We may decompose the polarization of the ROM into two parts: the density-dependent part and the Feynman (or, the vacuum) part. The Feynman part changes the sign of the correction to the energy functional as the charge-conjugate operator is acted on, and it would result in a very small contribution to the energy term linear in isospin asymmetry. This part is responsible for the usual CSB effect within the ROM picture as one performs the charge-conjugate operation. Here we do not see significant numerical contributions to the symmetry energy. However, the density-dependent part does not change sign for such an operation and mostly contribute to the symmetry energy term quadratic in isospin asymmetry. Secondly, the meaning of the in-medium CSB may concern the in-medium nucleon-nucleon interactions. In fact, if one discusses the in-medium nucleon-nucleon scatterings, the in-medium CSB has the content of the medium-induced ROM, and it is amplified dynamically by the incomplete cancelation between the proton and neutron loops in isospin-asymmetric matter.

Next, we discuss the causality issue in asymmetric nuclear matter. We examine the pressure by taking into account the rearrangement term. In addition to the contribution from the density dependence of the meson masses and coupling constants induced by the BR scaling, the rearrangement term in the CSLC includes several θ -entangled terms. In the CNL3, however, the rearrangement term is only from a single θ -related source. In Refs. [13, 14], a large θ close to 45° was obtained in isospin-asymmetric matter. In this case, unfortunately, the neglected rearrangement term actually dominates the pressure. More specifically, it gives the leading difference between the pressure and the energy density, i.e.,

$$p - \mathcal{E} \rightarrow \frac{m_0^{*2} - m_1^{*2}}{2m_\rho^{*4}} \frac{\sin 2\theta}{\cos^2 2\theta} (g_{n\omega}^* \rho_n - g_{p\omega}^* \rho_p)^2 \frac{\partial \theta}{\partial \rho}, \quad (23)$$

where m_0^* and m_1^* are taken their respective vacuum values in Refs. [13, 14]. It diverges to positive infinity for $\theta \rightarrow 45^\circ$ and $\partial\theta/\partial\rho > 0$ [13, 14]. This certainly violates the causality limit of $p \leq \mathcal{E}$. In fact, Eq.(23) remains finite for physical cases. The explicit violation of the causality indicates that the extremely large mixing angle obtained in Refs. [13, 14] is clearly inappropriate. It might be useful to comment here that the rearrangement term itself, necessarily required by the thermodynamic consistency, allows us to check the applicability or rationality of the methodology applied under the

extreme conditions of density and isospin asymmetry. To be more quantitative, in our treatment we examine the causality condition in pure neutron matter by displaying the relation between the energy density and the pressure in appendix B.

B. Results within the RPA

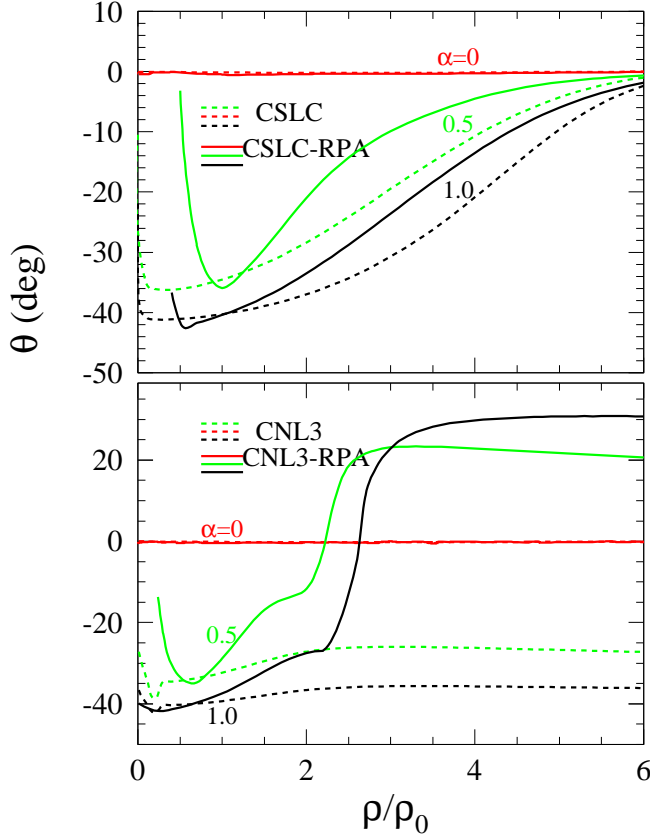


FIG. 5: (Color online) The mixing angle as a function of density for different isospin asymmetries. The upper panel is for the CSLC-RPA, and the lower is for the CNL3-RPA. For comparison, the results without the RPA correction are also exhibited.

The RPA equation contains both the real and imaginary parts of the polarizations. As we can see, the imaginary part goes away completely if the retardation effect is neglected, namely, by taking $q_0 = 0$. Thus, to keep the imaginary parts of the polarizations in the RPA equation, we have to account for the retardation effect. Here, we define the CSLC-RPA0 as the model similar to the CSLC0 but with the ROM calculated in the RPA. The model CSLC-RPA is the same as the CSLC-RPA0 but with $G_\rho = 2.8$ to reproduce the same symmetry energy at saturation density as the SLC. Similarly, we can define the models CNL3-RPA0 and CNL3-RPA (with $G_\rho = 3.36$) in reference to the CNL3 and NL3.

Fig. 5 shows the mixing angle with the CSLC-RPA (the upper panel) and CNL3-RPA (the lower

panel) for different isospin asymmetries. It is seen that the absolute value of the mixing angle with the CSLC-RPA reaches its maximum around the saturation density. Interestingly, this maximum is very close to the one obtained from the lowest-order ROM. Away from the maximum point, the magnitude of the mixing angle decreases compared to that from the CSLC. This indicates that the high-order contributions included in the RPA cancel partially the lowest-order ROM. Concretely, this partial cancellation occurs mainly between the longitudinal modes with and without the RPA correction since both the transverse mode of the lowest-order ROM and its RPA correction are small in the whole density region. It is known that the transverse mode of the lowest-order polarization is small compared to the longitudinal one. In the SLC model, the small value of the transverse RPA correction is mainly due to the following two facts. Firstly, the small transverse mode of the lowest-order ROM does not increase appreciably with the density because of the suppression added by the BR scaling. Secondly, the transverse eigencondition $\epsilon_T = 0$ can not be satisfied accordingly. However, the RPA correction in the NL3 model gives rise to a very different feature at high densities. As shown in the lower panel of Fig. 5, the mixing angle with the CNL3-RPA starts increasing from about twice the normal density and then becomes positive at density $\rho \geq 2.5\rho_0$. Similar to the case with the CSLC-RPA, the RPA correction to the longitudinal mode reaches its maximum in the vicinity of the saturation density and goes steadily without large changes at high densities in the CNL3-RPA calculations. Thus, this very different behavior from that obtained with the CSLC-RPA can only be due to the distinct property of the RPA correction to the transverse mode of the ROM with the CNL3-RPA. Within the CNL3-RPA, the small transverse mode of the lowest-order polarization increases with the density and the transverse eigencondition $\epsilon_T = 0$ can be satisfied at high densities ($\rho \geq 2.0\rho_0$). This then results in a large RPA correction to the transverse mode of the ROM, responsible for the sign change of the mixing angle. Similarly, at high densities the large difference between the CNL3 and CNL3-RPA results can be explained mainly by using the transverse mode property of the RPA polarization in the CNL3-RPA. Next, we examine the mixing angle in the low-density region. At very low densities ($\rho \leq 0.3\rho_0$), the mixing angle in highly isospin asymmetric matter can be shifted to positive values with both the CSLC-RPA and CNL3-RPA models. This shift is due to the reduced Pauli blocking on the various intermediate excitations (polarizations) at very low densities.

Fig. 6 depicts the parameter γ obtained with the CSLC-RPA and CNL3-RPA. Compared to the results shown in Fig. 2, the RPA correction shifts both the maximum value and its position moderately in the low-density region for both models. At high densities, larger effects of the RPA correction start to appear around $2\rho_0$. It is seen that the difference in γ between the CSLC-RPA and CNL3-RPA calculations also becomes more appreciable at high densities ($\rho \geq 2\rho_0$). These

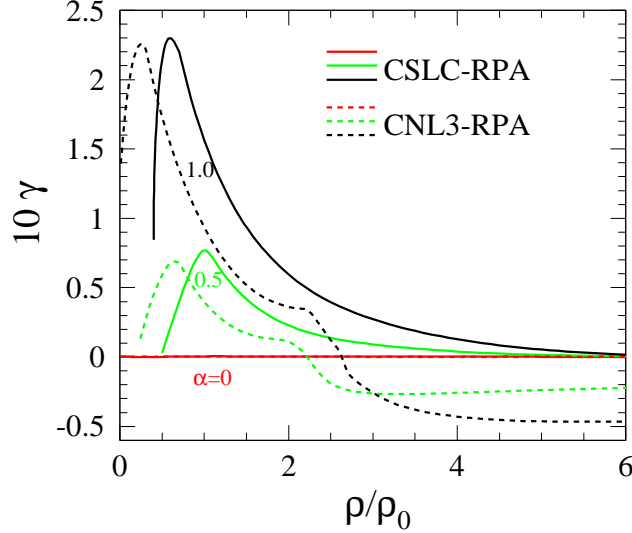


FIG. 6: (Color online) The parameter γ with the CSLC-RPA and CNL3-RPA for various isospin asymmetries.

observations are consistent with those from studying the mixing angle shown in Fig. 5.

Next, we turn to the RPA correction to the symmetry energy. Shown in Fig. 7 is a comparison of the symmetry energies obtained with the ROM with or without the RPA correction. We first examine in the upper panel effects of the ROM within the RPA on the symmetry energy with the CSLC-RPA0 and CSLC-RPA calculations. In the SLC model, consistent with the analysis for the mixing angle in the above, the RPA correction to the energy density is dominantly from the longitudinal mode. Comparing the results obtained with the CSLC-RPA0 and SLC, we can see that with the increasing density the medium-induced ROM with the RPA affects only slightly the symmetry energy. This is consistent with the effects on the mixing angle shown in Fig. 5. Moreover, by comparing the symmetry energy with the CSLC-RPA0 to that with the CSLC0, see Fig. 4, we see that the RPA correction to the lowest-order ROM is small at high densities. Since the RPA correction reaches its minimum at saturation density as shown earlier in Fig. 5, the bump is interestingly formed in the CSLC-RPA0 results. Noticing also that the RPA correction is almost negligible at saturation density, we can infer that the medium-induced ROM with the RPA modifies the symmetry energy as much as the lowest-order ROM at saturation density. When the symmetry energy at saturation density is constrained with the empirical value, it is then considerably softened at high densities. This softening is clearly seen in Fig. 7 by comparing the results obtained with the CSLC-RPA and SLC. At high densities, there is almost no difference between the symmetry energies obtained with the CSLC and CSLC-RPA. Furthermore, at subsaturation densities the symmetry energy with the CSLC-RPA is also softened with respect to the SLC due to the high-order correlations included in

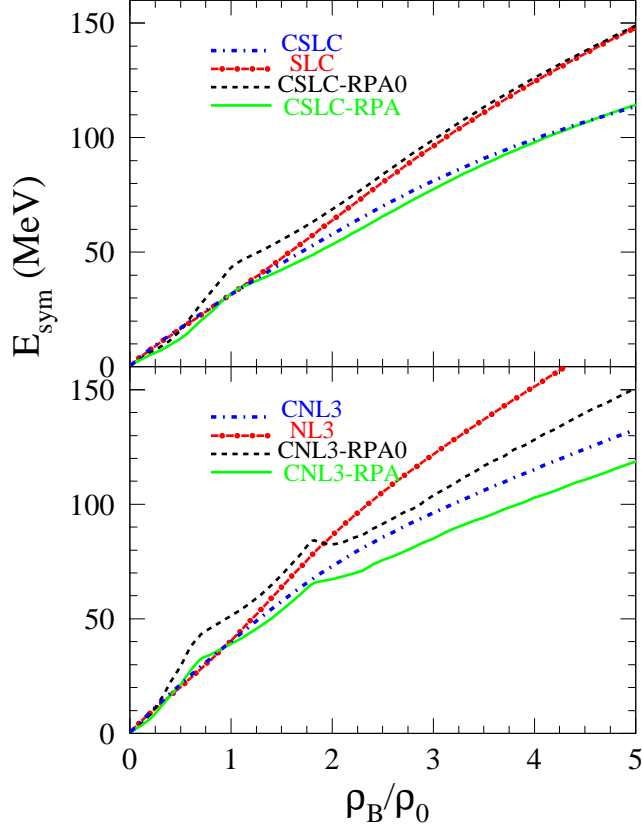


FIG. 7: (Color online) The symmetry energy as a function of density including the RPA corrections within the CSLC (upper panel) and CNL3 (lower panel). Here, the retardation effects are also included in the calculation within the CSLC and CNL3.

the RPA calculations.

In the lower panel of Fig.7, we compare results obtained with or without the RPA correction based on the NL3 parameter set. The CNL3-RPA0 and CNL3-RPA results display some noticeable bumpy structures. The bump formed at the lower density is associated dominantly with the RPA correction to the longitudinal mode of the ROM, since the transverse RPA correction is small at low densities. Thus, it can depend sensitively on the nonlinear self-interaction of the σ meson through the unperturbed propagator Δ , (see Eqs.(22),(A2)). In the nonlinear RMF model (such as the NL3), the σ -meson mass in the unperturbed propagator Δ becomes the effective mass due to its nonlinear self-interaction [32]. Once the self-interaction of the σ meson is neglected in the Δ , we find that the bump at the lower density is then shifted upwards and centralized around the saturation density, similar to the case with the CSLC-RPA0 which is free of the nonlinear meson self-interaction. As the nonlinear self-interaction of the σ -meson is necessarily included in the Δ in calculations with the NL3 model, the symmetry energy at subsaturation density is expected to be modified differently by the RPA compared to calculations with the SLC model. Noticeably, starting about $2\rho_0$ the

symmetry energy becomes softer in calculations with the RPA. Consequently, in the high-density region, the difference between the NL3 and CNL3-RPA0 results (lower panel) is significantly larger than that between the SLC and CSLC-RPA0 results (upper panel). This feature is consistent with that shown for the mixing angle and the parameter γ in Fig. 5 and 6, respectively. Again, this can be attributed to the different properties of the RPA correction to the transverse mode of the ROM in the CSLC-RPA0 and CNL3-RPA0 calculations. Moreover, the lowest-order ROM can largely soften the symmetry energy as seen clearly by comparing the results obtained with the NL3 and CNL3. This softening by the lowest-order ROM is dictated by the longitudinal mode, while the transverse mode plays only a minor role. We note that the RPA correction to the longitudinal ROM suppresses considerably the softening due to the lowest-order (longitudinal) ROM. Thus, it is worth stressing that in the nonlinear RMF model (NL3) the RPA correction to the transverse mode of the ROM plays a crucial role in softening the symmetry energy at high densities. Comparing the symmetry energy with the CNL3-RPA to that with the NL3, it is seen that the softening is very significant at high densities. Interestingly, the symmetry energy at high densities with the CNL3-RPA is comparable to that with the CSLC-RPA which features a typically soft symmetry energy at high densities.

In this work, we have only considered the medium-induced ROM and its impact on the vector meson properties and the symmetry energy. The in-medium $\sigma - \rho$ mixing may also affect the symmetry energy. However, its effect is expected to be much smaller than the ROM due to the small $\sigma - \rho$ polarization in the low-momentum region [44]. Nevertheless, a thorough investigation including the $\sigma - \rho$ mixing may be an interesting topic for a future work. It is also worth noting that in solving the RPA equation the Feynman parts of the polarizations except for the ROM are neglected. The neglected Feynman parts may be useful for studying the vacuum effect on the symmetry energy. This of course needs a lot more efforts in renormalized models. Finally, we also mention that the in-medium CSB effect on the EOS of symmetric nuclear matter is negligible. This finding is consistent with earlier conclusions as we discussed in the introduction.

IV. SUMMARY

In summary, using the RMF models with and without the BR scaling at high densities we studied the medium-induced ROM and its effects on the in-medium masses of the ρ and ω mesons and the density dependence of the symmetry energy in isospin-asymmetric dense nuclear matter. The mixing angle is obtained by reproducing the additional energy density from the $\omega - \rho$ conversion through the polarization diagram. We took into account the rearrangement term. Significantly different predictions from some earlier studies are made especially at high densities. We found that the symmetry energy is significantly softened instead of being stiffened at high densities by the medium-

induced ROM. The $\rho - \omega$ mass splitting due to the medium-induced ROM in highly neutron-rich matter is appreciable mostly at low densities and is small at high densities. While for the RMF model with the BR scaling, the $\rho - \omega$ mass splitting further vanishes at high densities. No large drop of the ρ meson mass is observed in asymmetric matter, contrary to some earlier studies by others. The medium-induced ROM is also studied with the RPA. The symmetry energy is significantly softened by the ROM in the RPA at both supra-saturation and sub-saturation densities. We also find that such a softening at sub-saturation densities due to the $\omega - \rho$ mixing can be partly suppressed by the nonlinear self-interaction of the σ meson.

Acknowledgement

We thank S. A. Chin, Lie-Wen Chen, and P. Krastev for helpful discussions. The work was supported in part by the US National Science Foundation Grants PHY-0652548 and PHY-0757839, the Research Corporation under Grant No. 7123 and the Texas Coordinating Board of Higher Education Grant No. 003565-0004-2007, the National Natural Science Foundation of China under Grant Nos. 10975033, 10575071 and 10675082, the China Jiangsu Provincial Natural Science Foundation under Grant No. BK2009261, the Knowledge Innovation Project of the Chinese Academy of Sciences under Grant No. KJXC3-SYW-N2, and the China Major State Basic Research Development Program under Contract No. 2007CB815004.

APPENDIX A: DIELECTRIC FUNCTIONS

Prior to giving the dielectric functions used in Eq.(22), we define the nucleon polarizations according to the Feynman rules [30, 45]:

$$\Pi^{ab}(q) = -i \int_{-\infty}^{\infty} \frac{d^4k}{(2\pi)^4} \text{Tr}[iG(k)\Gamma_a iG(k+q)\Gamma_b], \quad (\text{A1})$$

where the vertices $\Gamma_a = ig_{\sigma}^*$, $-iG_{\omega}^*\gamma_{\mu}$, and $-iG_{\rho}^*\tau\gamma_{\mu}$ for $a = \sigma, \omega$, and ρ , respectively. For the neutral ρ meson, the vertex is $-iG_{\rho}^*\tau_3\gamma_{\mu}$. For the nucleon propagator, we use the expression in Ref. [45]. With the general definition of polarizations, one can give the expression of the $\Pi_{\mu\nu}^{\rho\omega}$ in Eq.(12). The elements of the polarization matrices in Eq.(20) can also be written out explicitly according to the above definition.

The nucleon polarization for the vector meson can be appropriately decomposed into longitudinal and transverse modes such as in Eq.(13), (19) and (20). In the RPA equation for the nucleon polarization for the vector meson, the longitudinal and transverse dielectric functions in Eq.(22) are

given as:

$$\begin{aligned}
\epsilon_L = & (1 - \Delta\Pi^{\sigma\sigma})(1 - D_\omega\Pi_L^{\omega\omega})(1 - D_\rho\Pi_L^{\rho\rho}) - D_\omega D_\rho(1 - \Delta\Pi^{\sigma\sigma})(\Pi_L^{\rho\omega})^2 \\
& - \Delta D_\omega(1 - D_\rho\Pi_L^{\rho\rho})\frac{q^2}{\bar{q}^2}(\Pi_0^{\sigma\omega})^2 - \Delta D_\rho(1 - D_\omega\Pi_L^{\omega\omega})\frac{q^2}{\bar{q}^2}(\Pi_0^{\sigma\rho})^2 \\
& - 2\Delta D_\omega D_\rho\frac{q^2}{\bar{q}^2}\Pi_0^{\sigma\omega}\Pi_0^{\sigma\rho}\Pi_L^{\rho\omega}, \tag{A2}
\end{aligned}$$

and

$$\epsilon_T = (1 - D_\omega\Pi_T^{\omega\omega})(1 - D_\rho\Pi_T^{\rho\rho}) - D_\omega D_\rho(\Pi_T^{\rho\omega})^2. \tag{A3}$$

For simplicity, in the text we do not give the explicit expressions for all other polarizations except for the real part of the $\Pi^{\rho\omega}$ given since they can be found easily in literatures, e.g., see Refs. [30, 31, 46].

APPENDIX B: CAUSALITY CONDITION IN PURE NEUTRON MATTER AT HIGH DENSITIES

In order to examine the causality condition in our calculations, we display in Fig. 8 the pressure versus energy density for pure neutron matter. Comparing the results obtained using the CSLC and SLC, one sees that the in-medium CSB increases the pressure appreciably in both the low and high density regions. The same conclusion but to a lesser extent can be drawn from comparing results obtained using the CNL3 and NL3. Unfortunately, our numerical calculations, as illustrated in the inset for the high density tail, indicate that the causal condition $p \leq \mathcal{E}$ is broken with the CNL3 for $\rho \geq 7.2\rho_0$ (here, $r_0 = 0.16\text{fm}^{-3}$). These features displayed in Fig. 8 can be elaborated by virtue of the rearrangement term $-\Sigma_0 \rho$ in Eq.(10). The Σ_0 is given by

$$\Sigma_0 = \Sigma_{0\theta} + \Sigma_{0BR}, \tag{B1}$$

where

$$\Sigma_{0\theta} = -\frac{\partial\mathcal{E}}{\partial\theta}\frac{\partial\theta}{\partial\rho}, \quad \Sigma_{0BR} = -\sum_i \frac{\partial\mathcal{E}}{\partial\phi_i}\frac{\partial\phi_i}{\partial\rho},$$

with ϕ_i being the various scaling functions used in the SLC model [18]. For the CSLC calculations, since the θ approaches zero at very high densities, the Σ_{0BR} is little changed by the ROM. Thus, the increase of the pressure at very high densities with the CSLC compared to the SLC is due to the term $\Sigma_{0\theta}$. In pure neutron matter, the factor $\partial\mathcal{E}/\partial\theta$ in the $\Sigma_{0\theta}$ can be derived as

$$\frac{\partial\mathcal{E}}{\partial\theta} = -\frac{1}{2}\frac{(m_0^{*2} - m_1^{*2})\sin 2\theta}{\cos^2 2\theta}\left(\frac{g_{n\omega}^{*2}}{m_\omega^{*4}} - \frac{g_{n\rho}^{*2}}{m_\rho^{*4}}\right)\rho_n^2 + \left(\frac{1}{m_\omega^{*2}} - \frac{1}{m_\rho^{*2}}\right)g_{n\omega}^*g_{n\rho}^*\rho_n^2. \tag{B2}$$

In the CSLC, the first term dominates at very high densities because the BR scaling renders the effective masses of the vector mesons to be close to zero. With $\partial\theta/\partial\rho > 0$ and $\theta \rightarrow -0$ (see Fig. 2), the

rearrangement term $-\Sigma_{0\theta} \rho$ is positive, leading to the increase of the pressure at very high densities. On the other hand, since the masses of vector mesons are very large in the CNL3 compared to the CSLC, the violation of the causality limit at very high densities is dictated by the second term. We note here that the first and second terms of Eq.(B2) have opposite signs for negative θ values. While in the CNL3 calculations, unlike the CSLC case, one has $\partial\theta/\partial\rho < 0$ at very high densities. Thus, the second term of Eq.(B2) can increase the pressure and further violate the causality limit in the CNL3. It is useful to note that the reason for the causal breakdown here is different from the one in Refs. [13, 14]. In the latter, the inappropriate inducement produces a very large mixing angle close to 45° that is much larger than the one obtained here with the CNL3. Here, the violation of the causality limit is actually due to an inconsistent treatment. Considering the whole set of coupled equations for the propagators and self-energies, the Lorentz covariance is respected only approximately since we neglected the ROM loop-diagram correction to the self-energies. Consequently, this may lead to a formal violation of the Hugenholtz-Van Hove (HVH) theorem which is a conservation law ensuring the thermodynamical consistency. In isospin-asymmetric matter, the HVH theorem can be written as

$$\frac{\mathcal{E}}{\rho} + \rho \frac{\partial(\mathcal{E}/\rho)}{\partial\rho} = \frac{1}{2}[\mu_n(1 + \alpha) + \mu_p(1 - \alpha)], \quad (\text{B3})$$

where μ_n and μ_p are the neutron and proton chemical potentials, respectively. Since the nucleon chemical potentials are determined by the nucleon effective Fermi energies and self-energies, the neglect of the loop-diagram correction to the self-energies in evaluating the total energy density from the lagrangian (1) results in a formal violation of the HVH theorem. It is certainly a drawback of the CNL3 calculations. Nevertheless, as shown in Fig. 8, this violation is very weak and only visible at very high densities. Also, we notice that this situation is not very rare in calculations using models going beyond the mean field level. For instance, it is widely acknowledged that approaches such as the relativistic and non-relativistic Brueckner theories also unfortunately encounter similar problems in fulfilling accurately the HVH theorem [47–49].

In principle, a self-consistent treatment at least in the relativistic Hartree-Fock framework is needed to resolve the causality violation at very high densities. However, this is beyond the scope of the present work. Here, the loop-diagram correction to the self-energy is estimated to be tiny (roughly 2% in pure neutron matter), and the slight causal violation occurs only in highly isospin-asymmetric matter at very high densities. Therefore, the symmetry energy obtained in the vicinity of symmetric matter is not expected to be affected appreciably. Compared to the CNL3 calculations, the causality preservation with the CSLC is due to the fact that the mixing angle is almost zero at very high densities because of the BR scaling used. As shown in Fig. 8, the CSLC curve ends at the critical

density for the chiral restoration [18].

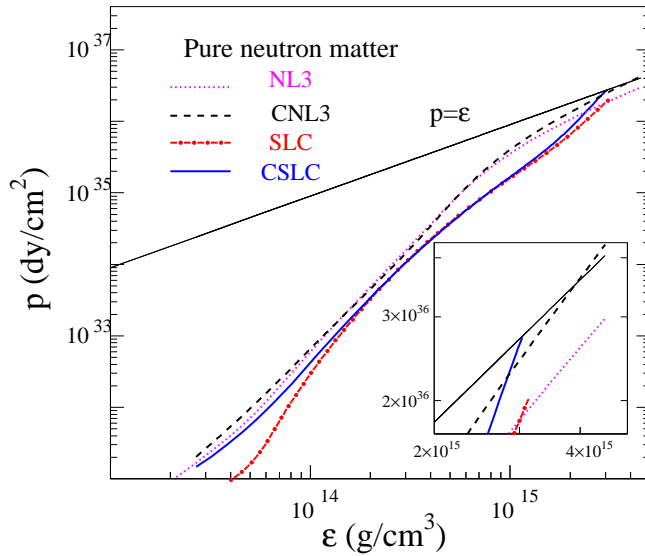


FIG. 8: (Color online) The pressure versus energy density in pure neutron matter. The inset shows the pressure within the small interval.

The features of Fig. 8 in the intermediate and low density regions can also be understood. In the intermediate density region, one has $\partial\theta/\partial\rho > 0$ within both the CNL3 and CSLC calculations. Thus the contributions from the first and second terms in Eq.(B2) cancel out to a large extent due to their opposite signs. As shown in Fig. 8, in the intermediate density region, the pressure is little modified by the θ -relevant rearrangement term. At low densities, however, a very distinct feature is exhibited by comparing the difference between the pressures obtained with the CSLC and SLC to that between those obtained with the CNL3 and NL3. In the SLC calculations, the pressure is increased significantly by the ROM, while it is just moderately increased in the NL3 calculations. Since their mixing angles are very close in this density region, the modification from the θ -relevant rearrangement term $\Sigma_{0\theta}$ is comparable for both the SLC and NL3 calculations. Thus, this large difference can only be due to the rearrangement term $-\Sigma_{0BR} \rho$ appearing only in the SLC parameter set.

-
- [1] G.A. Miller, B.M. K. Nefkens and I. Slaus, Phys. Rept. **194**, 1 (1990).
 - [2] R. Machleidt and H. Mütter, *topical review*, J. Phys. G **27**, 69 (2001).
 - [3] R. Machleidt and H. Mütter, Phys. Rev. **C63**, 034005 (2001).
 - [4] G. H. Bordbar, Int. J. Mod. Phys. **A18**, 3629 (2003); Int. J. Theor. Phys. **43**, 399 (2004).
 - [5] R. B. Wiringa, V. G. Stoks and R. Schiavilla, Phys. Rev. **C51**, 38 (1995).
 - [6] S.A. Coon, M.D. Scadron and P.C. McNamee, Nucl. Phys. **A287**, 381 (1977); S.A. Coon and R.C. Barrett, Phys. Rev. **C36**, 2189 (1987); S.A. Coon and M.D. Scadron, *ibid*, **C51**, 2923 (1995).
 - [7] P.C. McNamee, M.D. Scadron and S.A. Coon, Nucl. Phys. **A249**, 483 (1975).
 - [8] J. Piekarewicz and A. G. Williams, Phys. Rev. **C41**, R2462 (1993).
 - [9] M. Kimura, A. Suzuki and H. Tezuka, Phys. Lett. **B367**, 5 (1996).

- [10] A. K. Dutt-Mazumder, B. Dutta-Roy and A. Kundu, Phys. Lett. B**399**, 196 (1997).
- [11] A. K. Dutt-Mazumder, R. Hofmann and M. Pospelov, Phys. Rev. C**63**, 015204 (2000).
- [12] G. Q. Li and R. Machleidt, Phys. Rev. C**58**, 1393 (1998); *ibid*, C**58**, 3153 (1998).
- [13] M. Kimura, A. Suzuki, K. Suzuki and H. Tezuka Phys. Rev. C**56**, 3070 (1997).
- [14] A. Ishihara, A. Suzuki, M. Kimura and K. Suzuki, Phys. Rev. C**61**, 034004 (2000).
- [15] Y. Mori and K. Saito, Phys. Lett. B**552**, 21 (2003).
- [16] R. M. Aguirre and A. L. De Paoli, Phys. Lett. B**603**, 13 (2004).
- [17] Y. Muto and K. Saito, Phys. Lett. B**659**, 565 (2008).
- [18] W. Z. Jiang, B. A. Li and L. W. Chen, Phys. Lett. B**653**, 184 (2007).
- [19] W. Z. Jiang, B. A. Li and L. W. Chen, Phys. Rev. C**76**, 054314 (2007).
- [20] G. E. Brown and M. Rho, Phys. Rev. Lett. **66** (1991) 2720.
- [21] G. E. Brown, J. W. Holt, C.-H. Lee and M. Rho, Phys. Rep. **439**, 161 (2007).
- [22] G. Q. Li, C. M. Ko and G. E. Brown, Phys. Rev. Lett. **75** (1995) 4007.
- [23] M. Harada and K. Yamawaki, Phys. Rep. **381**,1 (2003).
- [24] M. Harada, hep-ph/0703238.
- [25] M. Binger and C.-R. Ji, Phys. Rev. D**60**, 056005 (1999).
- [26] H. Lenske and C. Fuchs, Phys. Lett. B**345**, 355(1995); C. Fuchs, H. Lenske and H. Wolter, Phys. Rev. C**52**, 3043 (1995).
- [27] C. J. Horowitz and B. D. Serot, Nucl. Phys. A**464**, 613 (1987).
- [28] A. Bouyssy, J.F. Mathiot, V. G. Nguyen and S. Marcos, Phys. Rev. C**36**, 380 (1987).
- [29] R. Brockmann and R. Machleidt, Phys. Rev. C**42**, 1965 (1990).
- [30] S. A. Chin, Ann. Phys. **108**, 301 (1977).
- [31] C. J. Horowitz and K. Wehrberger, Nucl. Phys. A**531**, 665(1991).
- [32] S. Reddy, M. Prakash, and J. M. Lattimer and J. A. Pons, Phys. Rev. C**59**, 2888(1999).
- [33] G.A. Lalazissis, J.König and P.Ring, Phys. Rev. C**55**, 540 (1997).
- [34] P. Danielewicz, R. Lacey and W. G. Lynch, Science **298**, 1592, (2002).
- [35] M. B. Tsang, et al., Phys. Rev. Lett. **92**, 062701 (2004).
- [36] L. W. Chen, C. M. Ko and B. A. Li, Phys. Rev. Lett. **94**, 032701 (2005).
- [37] B. A. Li and L. W. Chen, Phys. Rev. C **72** (2005) 064611.
- [38] G. Agakichiev et al., Phys. Rev. Lett. **75**, 1272 (1995).
- [39] M. Naruki et al., Phys. Rev. Lett. **96**, 092301 (2006).
- [40] D. Trnka et al., Phys. Rev. Lett. **94**, 192303 (2005).
- [41] W. Reisdorf et al. (FOPI Collaboration), Nucl. Phys. A **781**, 459 (2007).
- [42] Z.G. Xiao, B.A. Li, L.W. Chen, G.C. Yong and M. Zhang, Phys. Rev. Lett. **102**, 062502 (2009).
- [43] B. A. Li, Phys. Rev. Lett. **85**, 4221 (2000); *ibid*. **88**, 192701 (2002).
- [44] P. Roy, A. K. Dutt-Mazumder, S. Sarkar and J. Alam, J. Phys. G**35**, 065106 (2008).
- [45] B.D.Serot and J.D.Walecka, Adv. Nucl. Phys. **16**, 1(1986).
- [46] K. Lim, and C. J. Horowitz, Nucl. Phys. A **501**, 729(1989).
- [47] N. I. Kassis, J. Phys. G **6**, 205 (1980).
- [48] F. de Jong and H. Lenske, Phys. Rev. C **54**, 1488 (1996).
- [49] W. Zuo, I. Bombaci and U. Lombardo, Phys. Rev. C **60**, 024605 (1999).